THE JOURNAL OF BIOLOGICAL CHEMISTRY VOL. 291, NO. 10, pp. 5172–5184, March 4, 2016

Use of Cysteine Trapping to Map Spatial Approximations between Residues Contributing to the Helix N-capping Motif of Secretin and Distinct Residues within Each of the Extracellular Loops of Its Receptor*

Received for publication, November 21, 2015, and in revised form, January 5, 2016 Published, JBC Papers in Press, January 6, 2016, DOI 10.1074/jbc.M115.706010

Maoqing Dong[‡], Polo C.-H. Lam[§], Andrew Orry[§], Patrick M. Sexton[¶1], Arthur Christopoulos[¶1], Ruben Abagyan[§‖], and Laurence J. Miller[‡2]

From the [‡]Department of Molecular Pharmacology and Experimental Therapeutics, Mayo Clinic, Scottsdale, Arizona 85259, [§]Molsoft LLC, La Jolla, California 92037, [¶]Drug Discovery Biology, Monash Institute of Pharmaceutical Sciences and Department of Pharmacology, Monash University, Parkville 3052, Australia, and the [‖]Skaggs School of Pharmacy and Pharmaceutical Sciences, University of California San Diego, La Jolla, California 92037

Amino-terminal regions of secretin-family peptides contain key determinants for biological activity and binding specificity, although the nature of interactions with receptors is unclear. A helix N-capping motif within this region has been postulated to directly contribute to agonist activity while also stabilizing formation of a helix extending toward the peptide carboxyl terminus and docking within the receptor amino terminus. We used cysteine trapping to systematically explore spatial approximations between cysteines replacing each residue in this motif of secretin (sec), Phe^6, Thr^7, and Leu^{10}, and cysteines incorporated into the extracellular face of the receptor. Each peptide was a full agonist for cAMP, but had a lower binding affinity than natural hormone. These bound to COS cells expressing 61 receptor constructs incorporating cysteines in every position along each extracellular loop (ECL) and adjacent parts of transmembrane (TM) segments. Patterns of covalent labeling were distinct for each probe, with Cys^6-sec labeling multiple residues in the carboxyl-terminal half of ECL2 and throughout ECL3, Cys^7-sec predominantly labeling only single residues in the carboxyl-terminal end of ECL2 and the amino-terminal end of ECL3, and Cys^{10}-sec not efficiently labeling any of these residues. These spatial constraints were used to refine our model of secretin bound to its receptor, now bringing ECL3 above the amino terminus of the ligand and revealing possible charge-charge interactions between this part of secretin and receptor residues in TM5, TM6, ECL2, and ECL3, which can orient and stabilize the peptide-receptor complex. This was validated by testing predicted approximations by mutagenesis and residue-residue complementation studies.

The amino-terminal regions of natural peptide ligands for class B1 G protein-coupled receptors (GPCRs)[3] contain key determinants for biological activity and receptor specificity; however, a detailed understanding of how this region of these peptides might interact with and activate their receptors is unknown. Within the amino terminus of these peptide ligands are helix N-capping motifs that have been postulated to contribute directly to their agonist activity (1) while also stabilizing the carboxyl-terminal helical regions of the peptides that are known to dock within the receptor amino-terminal domains (2, 3). Indeed, this carboxyl-terminal helical conformation of the peptide ligands is critical for their proper docking into the cleft present within the amino-terminal domain of their receptors, an interaction that contributes substantial binding energy (2, 3). This key interaction likely also helps to direct the amino-terminal regions of these peptides toward the relevant core domains of their receptors.

The secretin receptor was the first member identified in this receptor family that includes several potentially important drug targets (4) and is prototypic of other members in every way (3). Its natural peptide ligand, secretin, is a 27-residue linear peptide that is also fully typical of the group of class B1 ligands (3). The current project utilized cysteine trapping to systematically explore spatial approximations for each of the helix N-capping motif residues within secretin, representing residues Phe^6, Thr^7, and Leu^{10}, and those residues within the core of the secretin receptor that could potentially contribute to this important binding pocket. We recently reported a similar approach to define spatial approximations with the more distal amino-terminal residues two and five within secretin (5). That effort supported the presence of this pocket, but the establishment of multiple disulfide bonds for each of the probes suggested that there was a dynamic component to the docking, and definition of more approximations would be necessary to refine our understanding.

Our understanding of the conformational diversity of class B GPCRs as well as the impact of peptide docking to these recep-

* This work was supported by the NIDDK of the National Institutes of Health (Grant DK046577). This work was also supported by the National Health and Medical Research Council of Australia Program Grant 1055134 and Project Grant 1061044, and by the Mayo Clinic. The authors declare that they have no conflicts of interests with the contents of this article. The content is solely the responsibility of the authors and does not necessarily represent the official views of the National Institutes of Health.

[1] Principal Research Fellows of the National Health and Medical Research Council of Australia.

[2] To whom correspondence should be addressed: Mayo Clinic, 13400 East Shea Blvd., Scottsdale, AZ 85259. Tel.: 480-301-4217; Fax: 480-301-8387; E-mail: miller@mayo.edu.

[3] The abbreviations used are: GPCR, G protein-coupled receptor; TM, transmembrane segment; GIP, glucose-dependent insulinotropic peptide; sec, secretin.

tors was substantially advanced recently with the use of multiple complementary approaches directed at the intact glucagon receptor (6). In that work, electron microscopy, hydrogen/deuterium exchange, molecular dynamics simulations, and complementary incorporation of cysteines to form disulfide bonds were used to describe closed and open conformations of that receptor based on the position of the receptor amino terminus relative to the receptor helical bundle domain. The most energetically favored conformation of the non-ligand-bound basal condition of the receptor was closed with the receptor amino terminus blocking the orthosteric agonist binding site. Based on previous kinetic studies with the parathyroid hormone receptor (7), it has been suggested that the peptide carboxyl terminus initiates the ligand docking process by occupying its cleft within the receptor amino terminus, preceding the functionally important docking of the ligand amino terminus. The recent glucagon receptor study (6) suggests that the ligand selects the open conformation of the receptor that lets this process occur and that this two-stage process can help to direct the biologically active peptide amino terminus toward its docking site high in the helical bundle (termed the J or junctional region). These proposed processes focus even more interest on the peptide ligand helical N-capping motif, since this resides between the part of the ligand that docks within the cleft in the receptor amino terminus and the part of the ligand known to confer biological activity by interacting with the helical bundle. The current approach should help to clarify the parts of the receptor that are spatially approximated with the ligand helical N-capping motif as this series of events might occur.

We have, therefore, developed additional probes in which cysteines were incorporated into each of the N-capping motif positions within secretin. Each of these analogues was a full agonist for cAMP, although each probe bound with lower affinity than that of the natural hormone. We applied these probes to the same extensive series of secretin receptor mutants in which the natural residues in each of 61 positions throughout the tops of transmembrane segments (TM) and extracellular loop (ECL) regions were replaced with cysteines that had been probed previously (5). These receptor constructs were expressed in COS cells, and the ligand probes were allowed to bind under conditions permitting the spontaneous formation of disulfide bonds.

Of note, the patterns of covalent labeling were distinct for each of the three probes. The position-six probe labeled multiple residues in the carboxyl-terminal half of ECL2 and throughout ECL3, whereas the position seven probe was more selective, predominantly labeling only a single residue at the carboxyl-terminal end of ECL2 and one residue at the amino-terminal end of ECL3. The position 10 probe did not efficiently label any of the residues in any of these regions. Receptor residues contributing to disulfide bond formation with the helix N-capping motif residues were distinct from the predominant sites of labeling previously observed with the position two and five cysteine probes (5). These sets of spatial approximation data were added to all previous experimentally derived constraints to refine our previous working model of the secretin-occupied secretin receptor (5). Predictions for spatial approximations made based on this model were further tested by receptor mutagenesis and complementary changes in residues within ligand and receptor. These help to validate this model and serve to extend our understanding of the molecular interactions that contribute to activation of this prototypic class B G protein-coupled receptor.

Peptide	Sequence
	1 5 10 15 20 25
Sec(1-27)	HSDGTFTSELSRLREGARLQRLLQGLV$_{NH_2}$
[C^{6},Y^{10}]sec(1-27)	HSDGT**C**TSE**Y**SRLREGARLQRLLQGLV$_{NH_2}$
[C^{7},Y^{10}]sec(1-27)	HSDGTF**C**SE**Y**SRLREGARLQRLLQGLV$_{NH_2}$
[C^{10},Y^{26}]sec(1-27)	HSDGTFTSE**C**SRLREGARLQRLLQG**Y**V$_{NH_2}$

FIGURE 1. **Primary structures of secretin analogues used in this study.** Shown are the amino acid sequences of natural human secretin(1–27) and its analogues, each incorporating a cysteine in positions 6, 7, or 10. Natural residues are illustrated in *gray*, whereas modified residues are illustrated in *black*.

Experimental Procedures

Materials—Amino acids for peptide synthesis were purchased from Advanced ChemTech (Louisville, KY), and Pal resin was from Sigma. Sodium ^{125}iodide was from PerkinElmer Life Sciences. Dulbecco's modified Eagle's medium (DMEM) and soybean trypsin inhibitor were from Invitrogen. Fetal clone II culture medium supplement was from Hyclone Laboratories (Logan, UT). Bovine serum albumin was from Serologicals Corp. (Norcross, GA). Polyethyleneimine (25 kDa linear) was from Polysciences (Warrington, PA). All other reagents were analytical grade.

Peptides—The cysteine-containing peptides were designed to incorporate a cysteine for disulfide trapping in positions 6, 7, and 10 of secretin that contribute to its helix N-capping motif. They represented analogues of human secretin(1–27) that included [Cys^{6},Tyr^{10}]secretin(1–27) (Cys^{6}-sec), [Cys^{7},Tyr^{10}]secretin(1–27) (Cys^{7}-sec), and [Cys^{10},Tyr^{26}]secretin(1–27) (Cys^{10}-sec) (Fig. 1). Both Cys^{6}-sec and Cys^{7}-sec incorporated a tyrosine to replace the leucine in position 10 for radioiodination (8), whereas Cys^{10}-sec incorporated a tyrosine to replace Leu^{26} for this purpose. All peptides were synthesized by manual solid-phase techniques using Pal resin and purified by reversed-phase HPLC as described (9) with their identities verified by matrix-assisted laser desorption/ionization-time-of-flight mass spectrometry.

Radioiodination—Cys^{6}-sec, Cys^{7}-sec, Cys^{10}-sec, and the secretin-like radioligand [Tyr^{10}]secretin(1–27) that was used in competition ligand binding assays were radioiodinated oxidatively using procedures previously established (10). In brief, ~15 μg of each peptide was incubated with 1 mCi of Na^{125}I in 0.1 M borate buffer (pH 9.0) and exposure for 15 s to the solid phase oxidant, *N*-chlorobenzenesulfonamide (iodination bead) (Pierce). The radioiodinated peptides were purified by reversed-phase HPLC to yield specific radioactivities of ~2000 Ci/mmol using procedures as described (9).

Receptor Constructs—The wild type human secretin receptor (CHO-SecR) stably expressed in Chinese hamster ovary (CHO) (11) was used for characterizing the binding affinities and biological activities of Cys^{6}-sec, Cys^{7}-sec, and Cys^{10}-sec. Cells were cultured at 37 °C in an environment containing 5% CO_2 on tissue culture plasticware in Ham's F-12 medium supplemented with 5% fetal clone II and were passaged approximately twice a week.

Wild type and a total of 61 previously characterized secretin receptor constructs incorporating cysteine replacements for natural residues in each of the positions of the three extracellular loops except for positions with a naturally occurring cysteine were transiently expressed in COS-1 cells (American Type Culture Collection, Manassas, VA) (5) and used in cysteine trapping studies with the Cys^6-sec, Cys^7-sec, and Cys^{10}-sec probes. In addition, we have prepared alanine mutation constructs of Trp^{265} (ECL2), Phe^{337} (top of TM6), and Glu^{352} (ECL3) as well as Arg^{278} (top of TM5), predicted in this study to interact with secretin amino-terminal residue His^1 (W265A, F337A, and E352A) and Asp^3 (R278A), respectively. We have also prepared a site mutation of Arg^{278} in the top of TM5, replacing this residue with cysteine (R278C). Trp^{275} in ECL2 was predicted to be far away from the amino-terminal region of secretin, and mutation of this residue to an alanine was prepared as a presumed negative control. These constructs were also transiently expressed in COS-1 cells. Cells were maintained in Dulbecco's modified Eagle's medium (Invitrogen) supplemented with 5% fetal clone II and studied 48 h after transfection.

Receptor Binding—The radioligand competition binding assay was used to determine the ability of Cys^6-sec, Cys^7-sec, and Cys^{10}-sec to compete for secretin radioligand binding to CHO-SecR cells. Assays were performed using whole cell binding in 24-well tissue culture plates. CHO-SecR cells were grown to ~90% confluence and were washed twice with Krebs-Ringers/HEPES medium (25 mM HEPES (pH 7.4), 104 mM NaCl, 5 mM KCl, 2 mM $CaCl_2$, 1 mM KH_2PO_4, 1.2 mM $MgSO_4$) containing 0.01% soybean trypsin inhibitor and 0.2% bovine serum albumin before being incubated with a constant amount of radioligand, ^{125}I-[Tyr^{10}]sec(1–27) (11 pM, ~20,000 cpm), and increasing concentrations (ranging from 0 to 1 μM) of each of the cysteine-containing secretin analogues for 60 min at room temperature. Cells were then washed twice with ice-cold Krebs-Ringers/HEPES medium containing 0.01% soybean trypsin inhibitor and 0.2% bovine serum albumin to separate free from cell-bound radioligand before cells were lysed with 0.5 M NaOH. Membrane-bound radioactivity was quantified with a γ-spectrometer. Nonspecific binding was determined in the presence of 0.1 μM secretin and represented <15% of total binding. Competition binding curves were analyzed and plotted using the non-linear regression analysis program in the Prism software suite v3.0. Binding kinetics were determined by analysis with the Ligand program of Munson and Rodbard (12). Characterization of the new site mutation constructs (W265A, W275A, R278A, R278C, F337A, and E352A) was performed, with data analyzed in a similar way.

Biological Activity Assays—A time-resolved fluorescence-based cAMP assay was used to examine the ability of Cys^6-sec, Cys^7-sec, and Cys^{10}-sec to stimulate cAMP responses in CHO-SecR cells. Approximately 90% of the confluent cells in 96-well plates were washed twice with phosphate-buffered saline (PBS) and stimulated with increasing concentrations (ranging from 0 to 1 μM) of secretin or each of the cysteine-containing secretin analogues in Krebs-Ringers/HEPES medium containing 0.01% soybean trypsin inhibitor, 0.2% bovine serum albumin, 0.1% bacitracin, and 1 mM 3-isobutyl-1-methylxanthine for 30 min at 37 °C. The reaction solution was then aspirated, and cells were lysed with 6% ice-cold perchloric acid for 15 min with vigorous shaking. The cell lysates were adjusted to pH 6 with 30% $NaHCO_3$ and assayed for cAMP levels in a 384-well white OptiPlate using a LANCE cAMP kit from PerkinElmer Life Sciences. The cAMP concentration-response curves were analyzed and plotted using the non-linear regression analysis routine in Prism v3.0 (GraphPad, San Diego, CA). Characterization of the new site mutation constructs (W265A, W275A, R278A, R278C, F337A, and E352A) was performed, with data analyzed in a similar way.

Cysteine Trapping—COS-1 cells grown in 24-well plates (~80% confluence) were transfected with wild type and all the 61 cysteine secretin mutants using the polyethyleneimine method as we have previously described (5). After washing once with PBS, cells were incubated for 1.5 h at room temperature with 200 μl of DMEM containing 5% fetal clone II and ^{125}I-Cys^6-sec or ^{125}I-Cys^7-sec or ^{125}I-Cys^{10}-sec (~100,000 cpm per well) in the absence or presence of 0.1 μM secretin. After the medium was aspirated, cells were washed once with ice-cold PBS and incubated for 45 min at room temperature on a shaker with 80 μl of SDS Laemmli sample buffer (13) with or without 0.1 M dithiothreitol (DTT). Cells were then scraped from the wells, and lysates were transferred to 1.5-ml microcentrifuge tubes where samples were briefly sonicated to break the sticky DNA. After the samples were resolved in a 10% SDS-polyacrylamide gel, the gel was dried, and bands of interest were visualized by autoradiography with band densitometry analyzed by the ImageJ software (National Institutes of Health, Bethesda, MD). The apparent molecular weights of the radioactive bands were determined by interpolation on a plot of the mobility of the appropriate ProSieve protein markers (Cambrex, Rockland, ME) *versus* the log values of their apparent masses. Lengths of exposure of the autoradiographs were ~6 days.

Molecular Modeling—All molecular modeling was conducted using a stochastic global energy and restraints optimization procedure for internal coordinates (14) with the ICM-Pro package version 3.7 (MolSoft LLC, San Diego, CA) using the protocol we previously described (5). The initial model of the amino-terminal domain of the human secretin receptor was generated using as template the x-ray structure of the amino terminus of the glucose-dependent insulinotropic peptide (GIP) receptor complexed with the GIP peptide (PDB code 2QKH; Ref. 15). A pentasaccharide $Man_3GlcNAc_2$ was attached to secretin receptor residues Asn^{51}, Asn^{79}, Asn^{85}, and Asn^{107} to mimic their glycosylated state. The initial conformation of the human secretin peptide was generated using the NMR structure of receptor-bound PACAP as template, and aligning this with GIP in the GIP-GIP receptor complex to determine its initial docking pose.

The initial pose did not satisfy all experimentally determined photoaffinity labeling constraints. The whole complex was, therefore, globally optimized in the presence of spatial approximation constraints coming from our extensive series of photoaffinity labeling experiments using the rat secretin receptor (16). The following restraints were applied (peptide residue to its labeled receptor residue): Phe^6 to Thr^4; Arg^{12} to Ala^6; Leu^{13} to Val^{104}; Glu^{15} to Glu^{19}; Gly^{16} to Leu^{100}; Arg^{18} to Leu^{14}; Gln^{20}

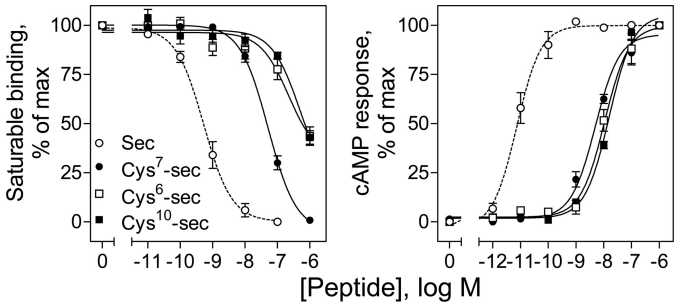

FIGURE 2. **Functional characterization of cysteine-containing secretin analogues.** *Left*, curves of increasing concentrations of secretin, Cys^6-sec, Cys^7-sec, and Cys^{10}-sec to compete for binding of the secretin radioligand, ^{125}I-[Tyr^{10}]sec(1–27), to CHO-SecR cells. Values represent the percentages of saturable binding, expressed as the means ± S.E. of duplicate values from a minimum of three independent experiments. *Right*, concentration-dependent intracellular cAMP responses in CHO-SecR cells to each of these peptides. Data points represent the means ± S.E. of data from three independent experiments performed in duplicate normalized relative to the maximal responses to secretin in these cells.

to His^2; Arg^{21} to Gln^{15}; Leu^{22} to Leu^{17}; Leu^{23} to Gln^{21}; Gln^{24} to Pro^{98}; Gly^{25} to Gln^{23}; Leu^{26} to Leu^{36}. Additionally, four fluorescence resonance energy transfer (FRET) distance constraints (17) were also incorporated. Twenty-five of the lowest energy complexes were retained.

The TM bundle was constructed using as the template the x-ray structure of the glucagon receptor helical bundle (PDB code 4L6R) (18). The peptide ligand-receptor amino-terminal domain complexes were then docked onto 200 diverse helical bundle domain models from 20 different TM bundles, each completed with 10 different loop conformations, in the presence of three additional photoaffinity labeling constraints involving the receptor core (peptide residue to its labeled receptor residue: His^1 to Phe^{339}; Ser^2 to Leu^{200}; Thr^5 to Phe^{350}) and 12 FRET distance constraints between the peptide and the transmembrane domain, as previously described (16, 19, 20). Seven constraints representing sites of disulfide bond formation from previous experiments were applied (peptide residue to its labeled receptor residue: Ser^2 to Trp^{274}, Ser^{340}, and Pro^{341}; and Thr^5 to Glu^{342}, Ile^{347}, Gln^{348}, and Phe^{351}) (5). Five additional constraints from the current disulfide bond formation experiment were also applied (peptide residue to its labeled receptor residue: Phe^6 to Asp^{343}, Ala^{344}, and Met^{345}; Thr^7 to Trp^{274} and Phe^{337}). All the resultant models were clustered, ranked by their ICM energetics and their health as established by PROCHECK and WHAT_CHECK evaluations (21). The best model from 200 independent docking runs was selected.

Results

Functional Characterization of Cysteine-containing Probes—The Cys^6-sec, Cys^7-sec, and Cys^{10}-sec analogues were characterized by competition ligand binding and cAMP assays to determine their ability to bind to secretin receptor-bearing CHO-SecR cells and to stimulate intracellular cAMP accumulation in these cells. As shown in Fig. 2, each of the three cysteine-containing secretin analogues had much lower affinity than natural secretin (IC_{50}: 0.6 ± 0.1 nM), with Cys^7-sec being higher than Cys^6-sec and Cys^{10}-sec (IC_{50} values: Cys^7-sec, 51 ± 10 nM; Cys^6-sec, 610 ± 240 nM; Cys^{10}-sec, 720 ± 140 nM). Although they had low affinity, these peptides were fully efficacious agonists, stimulating cAMP responses in CHO-SecR cells in a concentration dependent manner. Unlike the binding affinities, all three peptides had similar potencies in cAMP stimulation (EC_{50} values: Cys^6-sec, 18 ± 7 nM; Cys^7-sec, 5 ± 1 nM; Cys^{10}-sec, 16 ± 1 nM) but much lower than that of natural secretin (EC_{50}: 8.3 ± 2.0 pM). Full biological responses were observed with each of the probes when a small percentage of receptor binding sites were occupied.

Cysteine Trapping Data—As described above, each of the three cysteine-containing secretin analogues was a full agonist with reasonable binding affinity. We used each of them in cysteine trapping studies. Figs. 3–5 illustrate the labeling of each of the extracellular loop regions using cysteine-trapping with these probes. Representative autoradiographs in Fig. 3 show that none of the probes efficiently formed disulfide bonds with any of the residues within ECL1. In contrast, both the Cys^6-sec and Cys^7-sec probes formed significant disulfide bonds with residues in ECL2 (Fig. 4) and ECL3 (Fig. 5), whereas the Cys^{10}-sec probe did not form any significant disulfide bonds with any of those residues either (Figs. 4 and 5).

Figs. 4 and 5 include representative autoradiographs of both non-reduced and reduced gels in which the cysteine-containing probes were utilized to label each of the 61 cysteine-replacement ECL mutants along with the densitometric quantitation of the covalent receptor labeling observed with the Cys^6-sec and Cys^7-sec probes. As control, wild type secretin receptor was not covalently labeled (disulfide bond formed) by any of these probes under the experimental conditions (shown in Fig. 3). The patterns of labeling of receptor ECL2 (Fig. 4) and ECL3 (Fig. 5) residues by Cys^6-sec and Cys^7-sec were distinct from each other. Although Cys^6-sec predominantly labeled residues within the carboxyl-terminal half of ECL2 and throughout ECL3, Cys^7-sec labeled residues throughout ECL2 and within the amino-terminal region of ECL3. Quantitative analysis of labeling is shown in Table 1. Cys^6-sec covalently labeled cysteines in the positions of Ala^{344}, Met^{345}, Asp^{343}, Ser^{340}, Glu^{352}, and Pro^{341} with densitometry demonstrating intensities >50% that of the maximal signal attained with that probe in labeling any residue in any loop (A344C = 100%) (descending order) and Trp^{274}, Phe^{339}, Leu^{349}, Ala^{269}, and Asn^{268} with intensities between 25 and 50%. Cys^7-sec labeled Phe^{337} and Trp^{274} with intensities >50% that of the maximal signal with that probe (F337C = 100%) and Ala^{344} and Phe^{258} with intensities between 25 and 50%. These labeling intensities are expressed as relative intensities, as the absolute percentages of occupied receptors that were covalently labeled could not be determined due to nonspecific adsorbance of the probes to the membrane. No receptor labeling was observed with any of these mutants in the presence of DTT. Additionally, every condition in which covalent labeling of the receptor was observed was also studied in the setting of competition with 0.1 μM secretin to be certain of the saturable nature of the covalent labeling, with this eliminating all receptor labeling (data not shown).

Fig. 6 illustrates the receptor residues labeled by Cys^6-sec and Cys^7-sec compared with those labeled by Cys^2-sec and Cys^5-sec that were recently reported (5). This also provides additional evidence that many of the residues that are not covalently labeled with the currently studied probes are accessible for

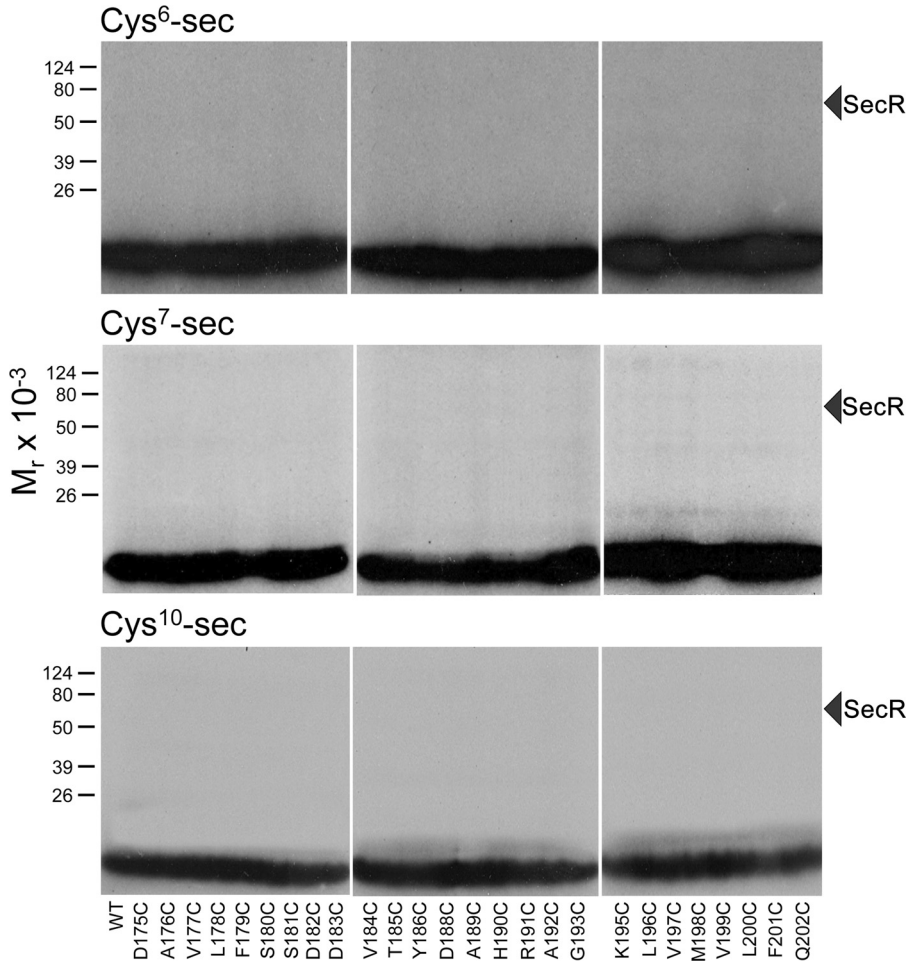

FIGURE 3. **Cysteine trapping experiments with secretin receptor ECL1 cysteine mutants.** Shown are typical autoradiographs of 10% SDS-PAGE gels used to separate the products of cysteine trapping of indicated ECL1 SecR mutants expressed in COS-1 cells by each of the noted cysteine-containing peptide probes. The position of electrophoretic migration of labeled SecR is identified. Because no significant receptor labeling was observed under non-reducing conditions, control autoradiographs of reducing gels that also did not show significant labeling are not shown. The signal observed at the *bottom of the gel* represents the radiolabeled probe that was bound to the membrane (nonspecific binding) and/or receptor (specific binding), surviving washing steps but not covalently bound to the receptor and, therefore, migrating with free probe. This signal has always been high in covalent labeling experiments with photolabile or cross-linkable radiolabeled secretin analogues, reflecting the tendency of such probes to adsorb to the membrane, yet the saturable nature of the receptor labeling has consistently been observed by competing with 0.1 μM secretin (data not shown).

labeling with other secretin analogue probes. This provides further assurance of proper folding of these receptor mutants.

Molecular Modeling—The current model used the recently released family B GPCR glucagon receptor helical bundle (PDB code 4L6R) as a template for the transmembrane domain. In addition to the distance constraints we had previously utilized, we have added new distance constraints representing the most efficient sites of covalent labeling from the current cysteine trapping results (Fig. 7, *A* and *B*). Although the current model shows a global orientation of the peptide-bound amino-terminal domain relative to the transmembrane domain, similar to that in our previous model, the new distance constraints resulted in tighter contact between the amino terminus of the secretin peptide and TM5, TM6, ECL2, and ECL3 regions of the secretin receptor, which allows us to make more specific predictions of peptide-receptor interactions.

Functional Characterization of Predicted Binding Site Mutation Constructs—The current best model predicts spatial approximations between His^{1} at the amino terminus of secretin and receptor residues Trp^{265} (ECL2), Phe^{337} (top of TM6), and Glu^{352} (ECL3) (Fig. 7*C*). Fig. 8 and Table 2 show the functional impact of replacing each of these residues with alanine. W265A neither bound secretin nor responded to secretin-stimulated cAMP production. An attempt at immunostaining intact cells with an amino-terminal region secretin receptor antiserum (22) was negative, suggesting that this mutant was trapped intracellularly and did not reach the cell surface (data not shown). F337A bound to secretin with an affinity 3.3-fold lower than wild type receptor. However, this mutation had more profound impact on secretin-stimulated cAMP production than on binding affinity, with a 266-fold reduction in potency compared with action on wild type receptor. Although E352A had similar affinity to the wild type receptor in binding secretin, this mutation also had a profound negative impact on secretin-stimulated cAMP production with potency 63-fold lower than that for the wild type secretin receptor. In brief, mutation of each of the two residues (Phe^{337} and Glu^{352}) predicted to interact with His^{1} of secretin impaired receptor function. In contrast, mutation of receptor residue Trp^{275} in ECL2 that was predicted to be

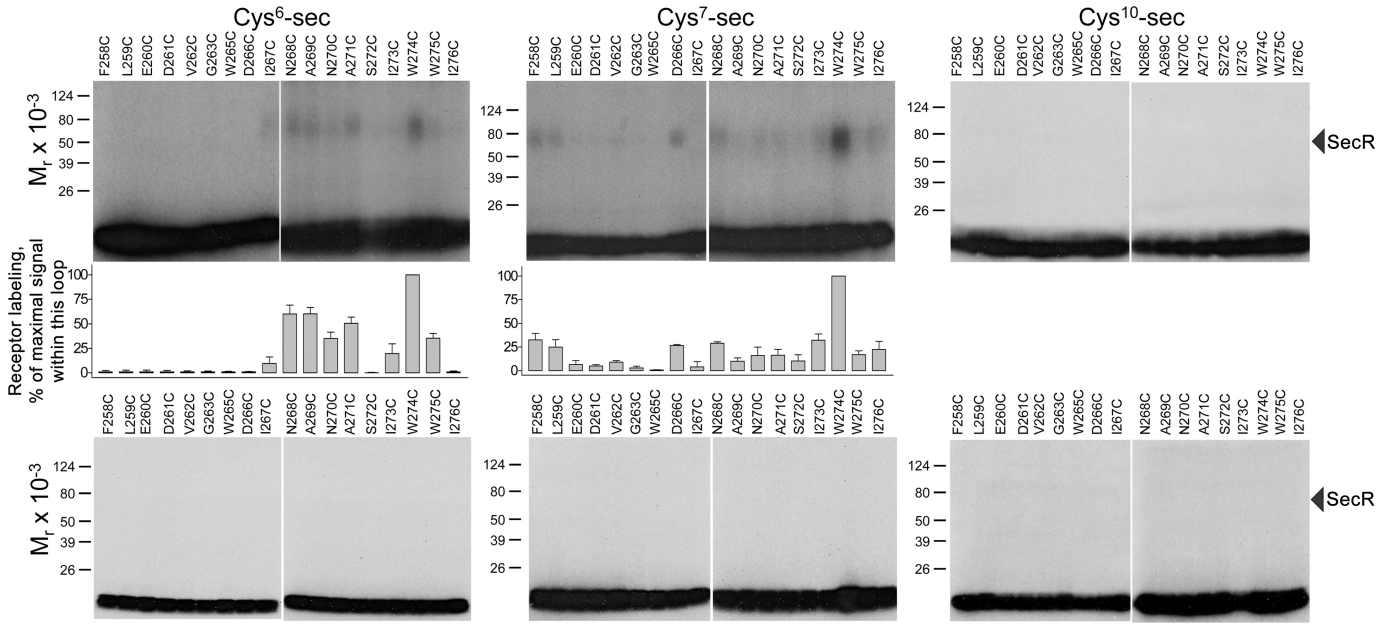

FIGURE 4. **Cysteine trapping experiments with secretin receptor ECL2 cysteine mutants.** Shown are typical autoradiographs of 10% SDS-PAGE gels used to separate the products of cysteine trapping of indicated ECL2 SecR mutants expressed in COS-1 cells by each of the noted cysteine-containing peptide probes. Shown are autoradiographs of gels run in the absence (*top*) and presence (*bottom*) of the reducing agent, DTT. Shown as well is the densitometric analysis of data from three similar experiments with the Cys^6-sec and Cys^7-sec probes. Quantitation of covalent labeling by Cys^{10}-sec is not shown because no significant labeling was observed with any of the mutants. The position of electrophoretic migration of probe-labeled SecR is identified, as in Fig. 3. The densitometrically determined intensities of labeling the receptor that are displayed represent the percentages of the signal for the maximal labeling of a residue within that particular loop by that probe.

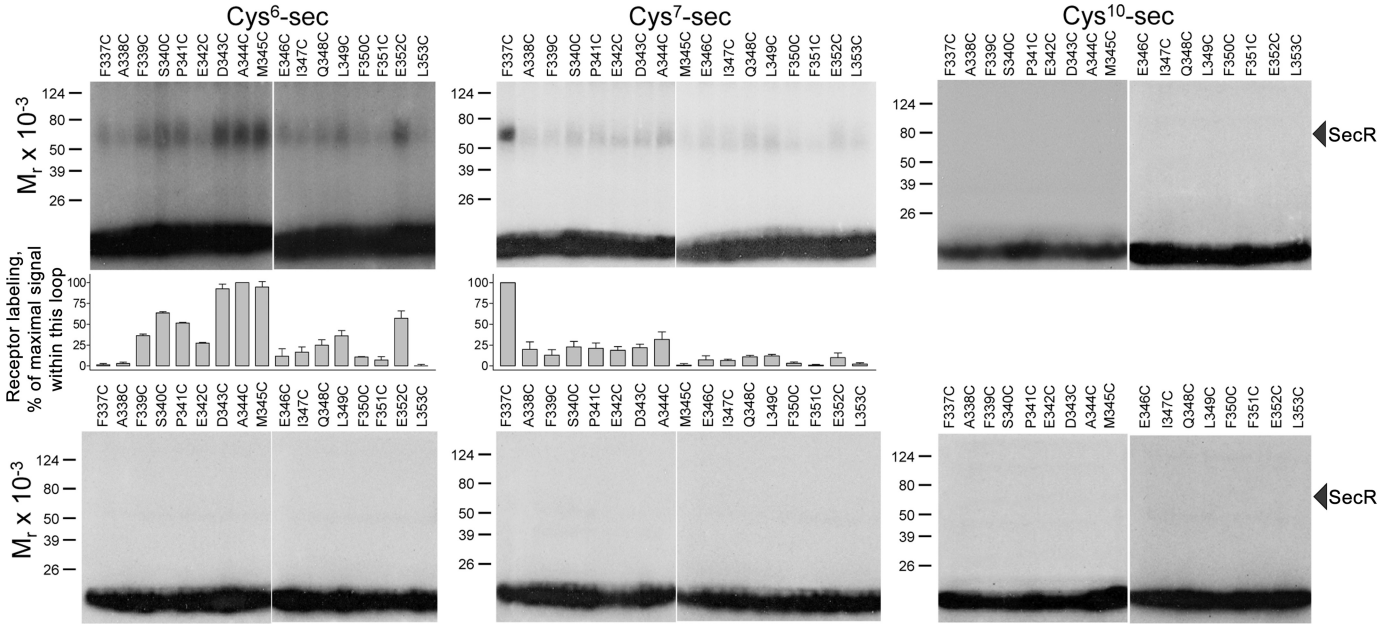

FIGURE 5. **Cysteine trapping experiments with secretin receptor ECL3 cysteine mutants.** Shown are typical autoradiographs of 10% SDS-PAGE gels used to separate the products of cysteine trapping of the indicated ECL3 SecR mutants expressed in COS-1 cells by each of the noted cysteine-containing peptide probes. Shown are autoradiographs of gels run in the absence (*top*) and presence (*bottom*) of the reducing agent, DTT. Shown as well is the densitometric analysis of data from three similar experiments with the Cys^6-sec and Cys^7-sec probes. Quantitation of covalent labeling by Cys^{10}-sec is not shown because no significant labeling was observed with any of the mutants. The position of electrophoretic migration of probe-labeled SecR is identified, as in Fig. 3. The densitometrically determined intensities of labeling the receptor that are displayed represent the percentages of the signal for the maximal labeling of a residue within that particular loop by that probe.

far away from the amino-terminal region of the peptide had no impact on receptor function.

The current best model also predicted spatial approximation between secretin amino-terminal residue Asp^3 and receptor residue Arg^{278} at the top of TM5 (Fig. 7*D*). Consistent with this, the R278A mutant exhibited a 7.1-fold reduction in potency for secretin to stimulate cAMP production compared with wild type secretin receptor (Fig. 8 and Table 2). In the current best model we observe a salt bridge between Asp^3 and receptor residue Arg^{278} (Fig. 7*D*). To further examine this, we prepared the

TABLE 1

Identification of receptor residues important for spatial approximation

Values represent the means ± S.E. of data from a minimum of three independent experiments. Intraloop labeling efficiency represents the intensity of labeling of each band as a percentage of the intensity of the band with the highest labeling intensity within each loop. Overall labeling efficiency represents the intensity of labeling of each band as a percentage of the intensity of the band with the highest labeling intensity using that probe in all three loops. Underlined values represent constructs with overall intensities >25% with those >50% marked with asterisks. ND, not detectable.

Receptor constructs	Cys^6-sec		Cys^7-sec	
	Intraloop labeling efficiency	Overall labeling efficiency	Intraloop labeling efficiency	Overall labeling efficiency
	% of max		*% of max*	
WT	ND	ND	ND	ND
ECL1				
D175C	ND	<1	ND	<1
A176C	ND	<1	ND	<1
V177C	ND	<1	ND	<1
L178C	ND	<1	ND	<1
F179C	ND	<1	ND	<1
S180C	ND	<1	ND	<1
S181C	ND	<1	ND	<1
D182C	ND	<1	ND	<1
D183C	ND	<1	ND	<1
V184C	ND	<1	ND	<1
T185C	ND	<1	ND	<1
Y186C	ND	<1	ND	<1
D188C	ND	<1	ND	<1
A189C	ND	<1	ND	<1
H190C	ND	<1	ND	<1
R191C	ND	<1	ND	<1
A192C	ND	<1	ND	<1
G193C	ND	<1	ND	<1
K195C	ND	<1	ND	<1
L196C	ND	<1	ND	<1
V197C	ND	<1	ND	<1
M198C	ND	<1	ND	<1
V199C	ND	<1	ND	<1
L200C	ND	<1	ND	<1
F201C	ND	<1	ND	<1
Q202C	ND	<1	ND	<1
ECL2				
F258C	1.6 ± 1.4	<1	32.5 ± 7.0	25.5 ± 5.5
L259C	1.3 ± 1.2	<1	24.8 ± 7.8	19.5 ± 6.5
E260C	1.4 ± 1.3	<1	6.5 ± 4.2	5.1 ± 3.4
D261C	1.5 ± 1.4	<1	4.7 ± 1.2	3.7 ± 1.0
V262C	1.3 ± 0.9	<1	8.9 ± 1.7	7.0 ± 1.4
G263C	1.2 ± 0.8	<1	2.8 ± 1.3	2.2 ± 1.2
W265C	1.8 ± 0.6	<1	0.5 ± 0.5	<1
D266C	1.0 ± 0.4	<1	26.5 ± 2.5	20.8 ± 2.4
I267C	9.6 ± 6.5	4.6 ± 5.7	3.9 ± 3.6	3.0 ± 2.5
N268C	60.1 ± 8.8	28.4 ± 6.8	28.8 ± 4.8	22.6 ± 4.4
A269C	60.2 ± 6.4	28.5 ± 6.0	9.9 ± 3.6	7.7 ± 3.3
N270C	35 ± 6.6	16.6 ± 6.1	15.9 ± 8.8	12.5 ± 7.7
A271C	50.5 ± 6.4	23.9 ± 4.9	16.1 ± 6.4	12.7 ± 5.8
S272C	1.0 ± 0.6	<1	10.2 ± 6.5	8.0 ± 6.2
I273C	19.6 ± 9.6	9.3 ± 8.8	21.3 ± 6.6	16.8 ± 6.3
W274C	100 ± 0	47.3 ± 0	100 ± 0	78.5 ± 0*
W275C	35.4 ± 4.8	16.7 ± 4.3	16.9 ± 4.2	13.3 ± 3.9
I276C	1.0 ± 0.8	<1	22.2 ± 8.8	17.4 ± 7.9
ECL3				
F337C	1.5 ± 1.3	1.5 ± 1.3	100 ± 0	100 ± 0*
A338C	2.9 ± 1.7	2.9 ± 1.7	19.9 ± 9.2	19.9 ± 9.2
F339C	36.4 ± 6.6	36.4 ± 6.6	13.0 ± 6.4	13.0 ± 6.4
S340C	63.7 ± 7.5	63.7 ± 7.5*	23.0 ± 5.6	23.0 ± 5.6
P341C	51.5 ± 9.9	51.5 ± 9.9*	21.3 ± 4.3	21.3 ± 4.3
E342C	20.4 ± 4.8	20.4 ± 4.8	18.8 ± 4.3	18.8 ± 4.3
D343C	92.6 ± 5.6	92.6 ± 5.6*	22.1 ± 3.7	22.1 ± 3.7
A344C	100 ± 0	100 ± 0*	32.0 ± 7.9	32.0 ± 7.9
M345C	94.8 ± 6.4	94.8 ± 6.4*	1.0 ± 0.9	1.0 ± 0.9
E346C	11.7 ± 7.6	11.7 ± 7.6	7.3 ± 4.7	7.3 ± 4.7
I347C	16.6 ± 6.3	16.6 ± 6.3	6.7 ± 1.9	6.7 ± 1.9
Q348C	24.0 ± 5.2	24.0 ± 5.2	11.0 ± 4.0	11.0 ± 4.0
L349C	36.3 ± 5.6	36.3 ± 5.6	12.0 ± 3.7	12.0 ± 3.7
F350C	10.8 ± 2.6	10.8 ± 2.6	3.2 ± 1.5	3.2 ± 1.5
F351C	7.2 ± 4.7	7.2 ± 4.7	1.0 ± 0.9	1.0 ± 0.9
E352C	57.3 ± 9.0	57.3 ± 9.0*	10.0 ± 4.6	10.0 ± 4.6
L353C	0.2 ± 0.2	<1	2.3 ± 1.6	2.3 ± 1.6

R278C mutant, attempting to stabilize the complex with appropriate cysteine-containing secretin analogues (Cys^1-sec and Cys^3-sec). This mutant bound secretin with similar affinity and exhibited similar potency secretin-stimulated cAMP responses to that of wild type secretin receptor (Fig. 9, *top panels*). When tested for binding and biological activity using Cys^1-sec, muta-

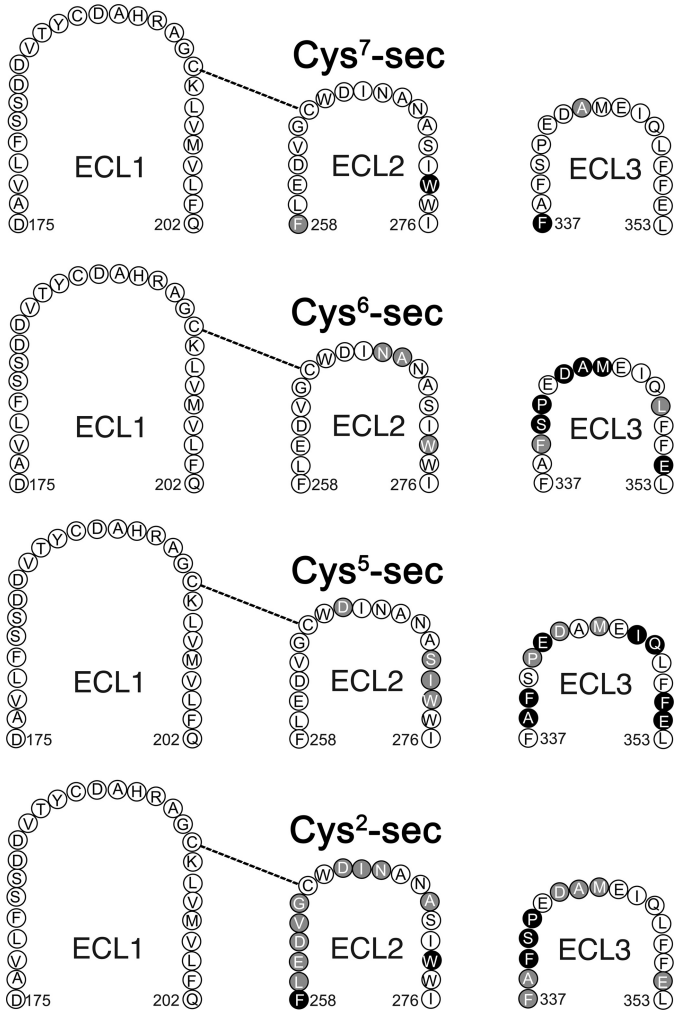

FIGURE 6. **Illustration of receptor residues important for spatial approximation.** Shown are schematic diagrams of three secretin receptor ECLs illustrating spatially approximated receptor residues for positions 7 (*top row*) and 6 (*second row*) of secretin identified in the current study and those for positions 5 (*third row*) and 2 (*bottom row*). Residues *highlighted in black circles* had overall labeling intensities of >50% of the maximal signal with that probe, whereas those *highlighted in gray* had labeling intensities of 25–50% (Table 1 and Ref. 5).

tion of Arg^{278} to a cysteine had no significant impact (Fig. 9, *middle panels*). Interestingly, this cysteine mutation resulted in a 6.4-fold increase in affinity of binding Cys^3-sec compared with that at the wild type secretin receptor (Fig. 9, *bottom panels*). However, although stabilizing the binding pose, the conformation did not facilitate biological activity, with a lower response than wild type receptor (Fig. 9, *bottom panels*).

Discussion

The helix N-capping motif that is highly conserved within the natural peptide ligands for the class B1 G protein-coupled receptors has been the focus of substantial interest in recent years (1, 23). In addition to its likely role to stabilize the helical conformation extending through the mid-region and carboxyl-terminal region of these peptides, it has been postulated to play a direct role in activation of these receptors and possibly even to serve as a structural lead to small molecule agonist development (1, 23). However, little is known about the site of docking this motif and the receptor residues that might be adjacent to it as docked in an activated ligand-receptor complex. Replacement of the residues that contribute to this motif with a photolabile residue for photoaffinity labeling has been attempted (24, 25), but there has been concern that the requirement for a relatively large and bulky hydrophobic moiety that is necessary to achieve photoactivation might have provided misleading insights into natural spatial approximations that are critical for agonist activity. In the current work, therefore, we replaced these residues with smaller cysteine residues that could be used to establish relatively short and geometrically defined disulfide bonds with cysteine residues in the receptor having the proper spatial relationship. By incorporating cross-linkable cysteine residues into every possible position at the top of transmembrane segments and into each of the extracellular loops, global screening could be achieved.

This approach also provides the advantage of probing spatial approximation that might exist at any stage along the dynamic process of ligand docking and conformational change in the ligand-receptor complex that is believed to occur. This is different from intrinsic photoaffinity labeling approaches in which spatial approximation can be established at a single point in time after stable ligand docking using photolysis. We know from very recent observations with the glucagon receptor (6) that the holo-receptor assumes a variety of conformations spanning from the dominant closed conformation with the receptor amino terminus covering the top of the helical bundle, likely occluding the orthosteric peptide ligand binding site, and interacting with all three extracellular loop regions at the top of the helical bundle, to an open conformation with the receptor amino terminus perpendicular to the membrane surface that can be stabilized by a bound peptide ligand (6). It was proposed that the natural peptide ligand could select this open conformation, binding first to the cleft in the receptor amino terminus and then subsequently to the J region high in the helical bundle that is likely responsible for biological activity (6). The helix N-capping motif within the natural ligand is positioned between the parts of the ligand that are known to dock within the receptor amino terminus and that are most critical for biological activity. This is clearly a site of considerable dynamic change in conformation and possible important spatial approximations with the receptor. Another possible explanation for the promiscuity of cysteine labeling involves local unfolding or misfolding in a small percentage of receptors. Although this cannot be ruled out, the ability to accommodate these experimentally derived spatial approximations within a credible molecular model provides some assurance that these are meaningful.

Indeed, in our current series of studies, each component of the helix N-capping motif yielded a distinct set of disulfide bonds. Of interest, the position 10 probe did not yield any demonstrable disulfide bonds at all despite having binding affinity at least as high as the other probes and being fully biologically active. This is consistent with the side group of that residue establishing a hydrophobic interaction with the side group of residue five as part of the N-capping motif (1, 23). It might, therefore, play a role in internal stabilization of such a motif rather than being available to interact directly with the

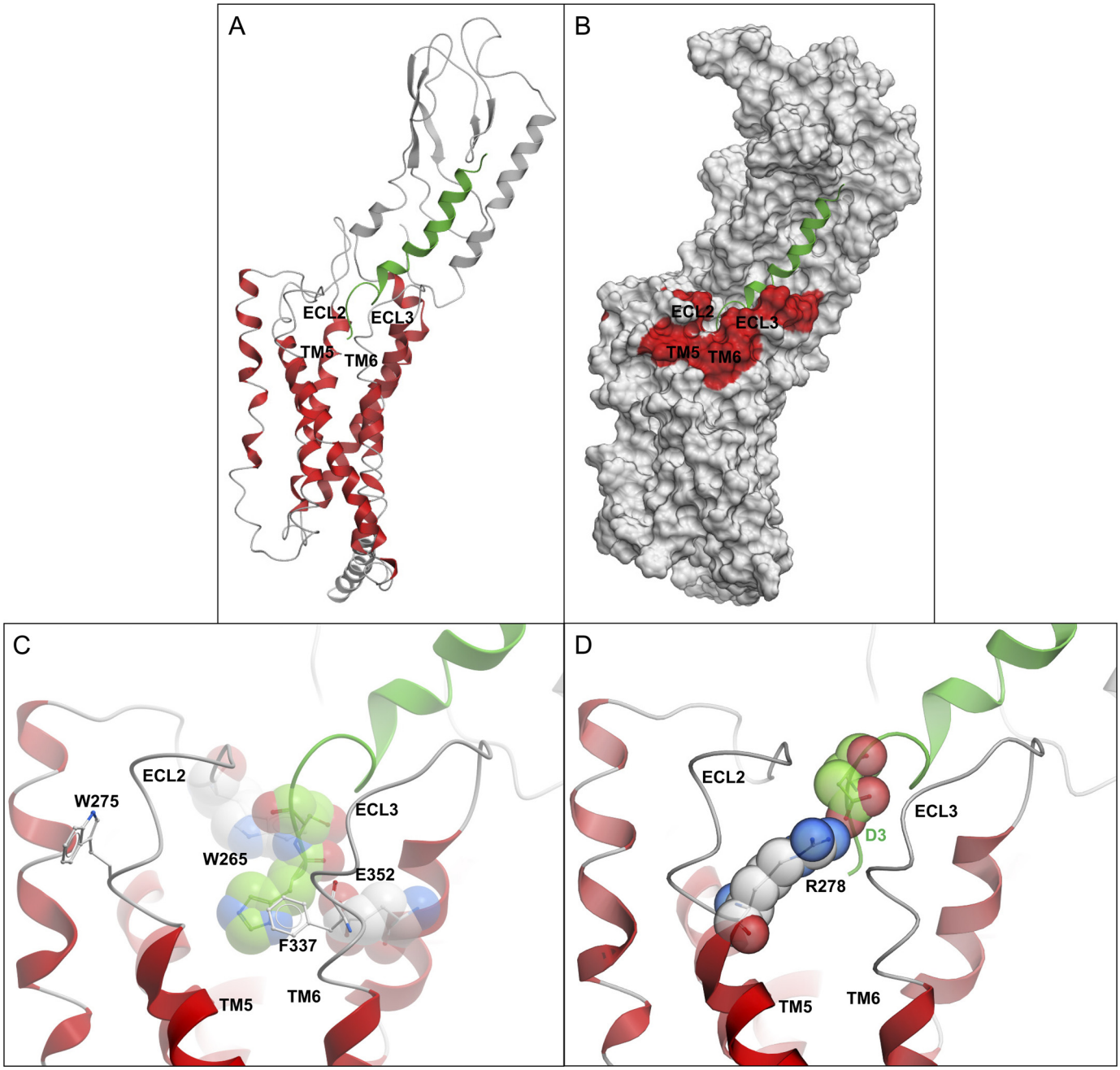

FIGURE 7. **Predicted residue-residue spatial approximations within the secretin-occupied secretin receptor model.** *A*, the most energetically favorable secretin-receptor model is shown. Receptor TM helices are colored *red*, and secretin is shown in *green ribbon* representation. Note the close interaction between the secretin amino terminus and ECL2, ECL3, TM5, and TM6. *B*, a surface representation of the secretin-receptor model is shown, and residues labeled by Cys^{6}-sec and Cys^{7}-sec are *shaded red*. *C*, His^{1} and Ser^{2} at the amino terminus of secretin (*green CPK carbon spheres and sticks*) are shown to have spatial approximation with Trp^{265} (ECL2), Phe^{337} (TM6), and Glu^{352} (ECL3). Trp^{275} was mutated as a negative control and is also highlighted. *D*, a salt bridge is formed between secretin Asp^{3} (*green carbon CPK sphere and sticks*) and receptor residue Arg^{278} (TM5). *CPK*, Corey-Pauling-Koltun.

receptor. It was also interesting that the position seven probe yielded only two sites of efficient bond formation, in residues Trp^{274} at the top of transmembrane segment five and Phe^{337} at the top of transmembrane segment six, both of which can be positioned relatively close to each other in space as well as simultaneously forming a complex with a single residue within a ligand docked into the helical bundle. The model predicts that Phe^{337} makes π-π stacking with His^{1} of the peptide at the floor of the pocket, and Trp^{274} points away, allowing Arg^{278} to make a key charge-charge interaction. Of note, both of these receptor residues are positioned adjacent to each other in the TM bundle. In the model, Thr^{7} of the peptide is sandwiched between two hydrophobic residues (Ile^{267} and Leu^{349}). In the classical N-capping motif, the side group of the threonine residue in position seven points away from the motif and could easily point toward a stable site of interaction with both of these residues within the receptor. We utilized this set of approximations as key to modifying our previous molecular model of the secretin-occupied secretin receptor. The position six probe, like the position two and position five probes studied in analo-

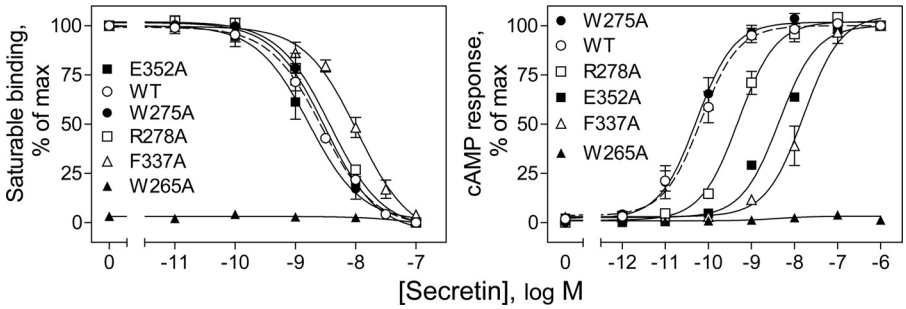

FIGURE 8. **Functional characterization of secretin receptor mutants.** *Left*, curves for increasing concentrations of secretin to compete for binding of a constant amount of radioligand, ^{125}I-[Tyr^{10}]sec(1–27), in COS-1 cells transiently expressing wild type (*WT*) and the indicated alanine mutant secretin receptor constructs. Values represent the percentages of saturable binding, expressed as the means ± S.E. of duplicate values from a minimum of three independent experiments. *Right*, concentration-dependent intracellular cAMP responses in response to secretin in these cells. Data points represent the means ± S.E. of three independent experiments performed in duplicate, normalized relative to the maximal responses in these cells.

TABLE 2

Binding and biological activity characteristics of wild type and mutant secretin receptors expressed in COS-1 cells

Values represent the means ± S.E. of a minimum of data from three independent assays performed in duplicate. Two-tailed *t* tests were performed to determine the significance of differences using Prism ver. 5 (GraphPad Software, San Diego, CA). ND, not determined.

Receptor constructs	Secretin binding		Intracellular cAMP response	
	K_i	B_{max}	EC_{50}	E_{max}
	nM	*Binding sites/cell × 10^3*	*nM*	*pmol/10^6 cells*
WT	2.8 ± 0.3	157 ± 16	0.07 ± 0.03	193 ± 55
W265A	ND	ND	ND	ND
W275A	3.4 ± 0.2	53.8 ± 4.7[a]	0.06 ± 0.02	189 ± 47
R278A	2.9 ± 0.6	66.2 ± 11.2[a]	0.5 ± 0.1[a]	202 ± 50
R278C	3.8 ± 0.5	78.2 ± 12.2[a]	0.1 ± 0.02	182 ± 48
F337A	9.2 ± 0.5[a]	46.6 ± 9.0[a]	18.6 ± 5.1[a]	188 ± 56
E352A	2.2 ± 0.6	55.5 ± 5.6[a]	4.4 ± 0.3[a]	199 ± 42

[a] Values significantly different from that of WT receptor ($p < 0.01$).

gous manner previously (5), formed multiple disulfide bonds with residues scattered throughout extracellular loops two and three. These spatial approximation constraints were also utilized in the evolving molecular model, although they were used as softer constraints that could have been more dynamically active and less stable as docked.

Although the probe with cysteine in position seven labeled only two receptor residues with high relative intensity (>50% of the maximal signal attained with that probe for a residue in any loop; A344C = 100%), the probe with cysteine in position six labeled at least six residues with similar high relative intensity, with all of these within ECL3 (F337C = 100%). Diffuse loop three labeling had also been observed with the position two and five probes previously (5). With these new insights it became clear that we had to modify the conformation and location of this loop in our most recent molecular model (5) to satisfy all of these experimentally derived constraints. The best way to accommodate these was to bring this loop over the amino terminus of the docked ligand as a "cover" for this portion of the ligand. It is noteworthy that this also means that ECL3 adjusts to provide a surface to potentially interact with the base of the receptor amino-terminal domain. Indeed, such an interaction between these two domains was proposed recently for the glucagon receptor (26), where modifying residues within ECL3 was postulated to disrupt such an interaction and an antibody known to bind to the top face of the receptor amino terminus lost its inverse agonist action. In other G protein-coupled receptors, extracellular loops have been found to provide an analogous "lid" function above an agonist ligand (27).

Although high resolution crystal structures have been solved for a series of intact G protein-coupled receptors (28), until quite recently these have all been in the class A family that has been predicted to be quite distinct from those receptors in the class B family (29). Our best insight into the class B structure came from the crystallization of the extracellular amino-terminal domains of several members of the B1 group (30, 31), some of these also including complexed peptide ligands (30, 31). Indeed, these observations have confirmed the presence of a highly conserved conformational motif, called a "sushi motif," which is formed by three intradomain disulfide bonds linking two antiparallel β sheet regions and various loops as well as a less consistent amino-terminal helix (30, 31). This structure provides a hydrophobic cleft for the docking of the carboxyl-terminal region of the natural peptide ligands in α-helical conformation (32). The first two crystal structures of isolated helical bundles of the glucagon and corticotropin releasing factor-1 receptors were finally reported in 2013, confirming differences that had been predicted from the helical bundles of class A GPCRs (18, 33). It is important to note that the orientation of the receptor amino-terminal domain relative to its core transmembrane domain of the class B GPCRs is still poorly understood, as demonstrated by a highly diverse set of proposed holoreceptor structures (5, 30). Adding to this uncertainty is the prediction that the helical bundle of the class B G protein-coupled receptors will be quite different from that of the class A receptors, now well defined in the crystal structures (18, 33).

The helical bundles of the glucagon and corticotrophin releasing factor-1 receptors exhibit a more open cavity in the extracellular side of the bilayer, whereas the intracellular face of the bundles was much like that of the class A receptors. Indeed, with receptors in both major families binding to and activating the same set of heterotrimeric G proteins, this seems quite logical. Extrapolating from this, one might also predict that the critical movements of transmembrane segments six, seven, and five that have now been consistently observed in the class A receptors that are associated with the activated state (34–37) will also be required for the class B receptors. Perhaps the large open cavity high in the helical bundle helps to explain why it has been so difficult to develop high affinity and high potency small molecule agonists for the class B G protein-coupled receptors and why the lead compounds that have been identified in high throughput screening efforts for the same receptor (example of

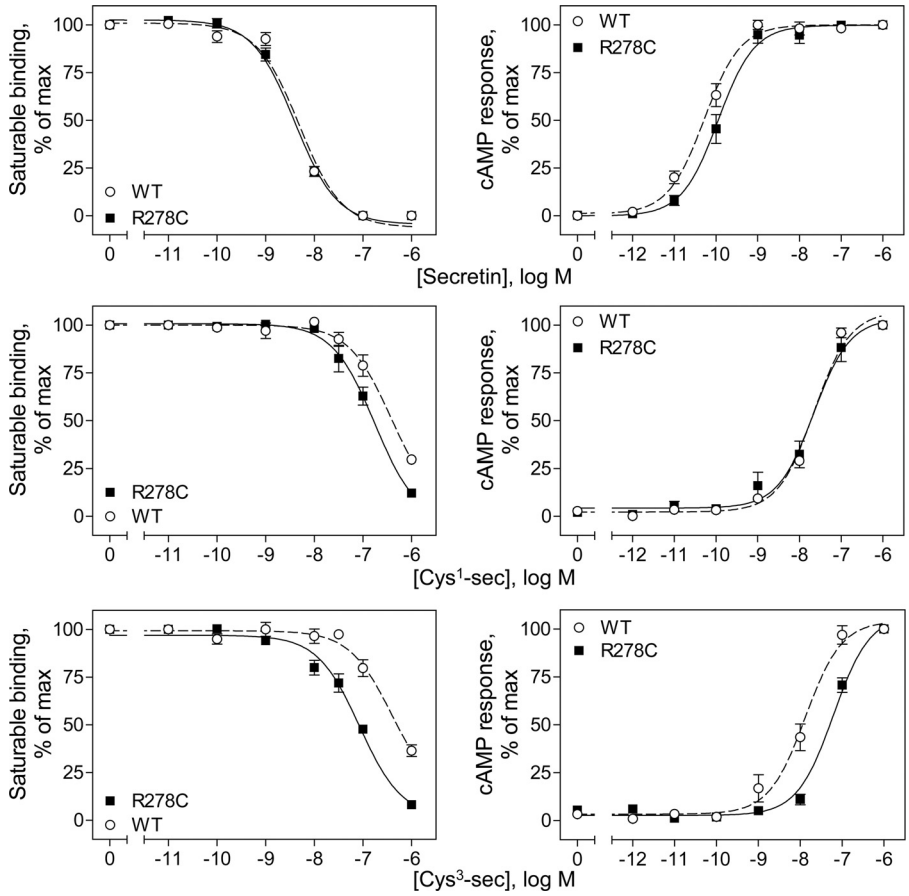

FIGURE 9. **Complementary mutagenesis data.** *Left*, curves for increasing concentrations of secretin (*top*), Cys^1-sec (*middle*), and Cys^3-sec (*bottom*) to compete for binding of a constant amount of radioligand, ^{125}I-[Tyr^{10}]sec(1–27), in COS-1 cells transiently expressing wild type (*WT*) and R278C mutant secretin receptor constructs. Values represent the percentages of saturable binding, expressed as the means ± S.E. of duplicate values from a minimum of three independent experiments. *Right*, concentration-dependent intracellular cAMP responses in response to secretin (*top*), Cys^1-sec (*middle*) and Cys^3-sec (*bottom*) in these cells. Data points represent the means ± S.E. of three independent experiments performed in duplicate, normalized relative to the maximal responses in these cells.

small molecule GLP-1 receptor agonists) may have such diverse structures (38). A better understanding of the docking of the amino terminus of a natural peptide ligand for the secretin receptor should help provide more insight into the molecular basis for activating a prototypic receptor in this family.

Indeed, it is quite interesting that the most specific spatial approximations determined in this work are with residues at the top of transmembrane segments five and six. These seem to be ideal sites to provide tension on these critical segments to transmit changes in conformation at the G protein-coupling interface. Receptor mutagenesis and photoaffinity labeling studies of the secretin receptor have supported important roles for these regions as well (5, 19, 20). This theme has been further supported by mutagenesis and photoaffinity labeling of other closely related receptors in this family (20, 32).

The results of the current cysteine trapping efforts, focused on the residues predicted to contribute to the helix N-capping motif, are consistent with the presence of such a motif in the secretin peptide as it is bound to its receptor. They also provide new focus on the residue in the second position of this motif, Thr^7 in secretin, because of the limited and focused nature of its covalent bonding pattern and the sites of those bonds. However, the relative absence of selectivity of the disulfide bonds observed now to be formed through the residue in position six and observed recently with residues in positions two and five (5) may indicate less specificity to their interactions and greater dynamic motion of these positions relative to the receptor as the peptide docks. Indeed, structure-activity series for residues in the amino terminus of secretin have indicated that a variety of residues that can support biological activity (39–41). This could suggest that the most important role of the helix N-capping motif is in stabilizing the helix rather than its having a "structural lead" role in drug development.

The floor of the secretin binding site within the TM bundle is predicted to comprise residues Ile^{277} (TM5), Ile^{205} (TM3), and Tyr^{334} (TM6) with Trp^{265} in ECL2 and Phe^{337} in the top of TM6 above the amino terminus of the peptide ligand. The α-amino group of the amino-terminal His^1 residue of secretin is predicted to make a salt bridge with Glu^{352} in ECL3. Indeed, alanine replacement of Phe^{337} resulted in a 3.3-fold loss in binding affinity and a 266-fold loss in secretin-stimulated cAMP production. Alanine replacement of Glu^{352} did not yield significant change in binding affinity, but it resulted in a 63-fold loss in secretin-stimulated cAMP production. Unfortunately, W265A was not detectable on the cell surface, so we were unable to test its function.

The model also suggests that secretin residue Asp^3 is closest to Arg^{278} in the top of TM5, likely representing a charge-charge

interaction. Although alanine replacement of this residue did not yield significant change in binding affinity, it resulted in a 7.1-fold reduction in secretin-stimulated cAMP production. Most interesting is that cysteine replacement of Arg^{278} that provided an acceptor for a new disulfide bond with Cys^3-sec resulted in a 6.4-fold increase in binding affinity, although this did not lead to paralleled enhancement of biological activity. This confirmed the likely close spatial approximation between position 3 of secretin and Arg^{278} of the receptor. It should be mentioned that previous mutagenesis studies showed that Asp^3 of secretin might be close to Tyr^{128} in the juxtamembranous region of the receptor amino-terminal domain (42), Arg^{166} in TM2, and Lys^{173} and Asp^{174} in ECL1 (43), whereas Asp^3 of VIP might be close to Arg^{188} and Lys^{195} in ECL2 of VPAC1 (44) and Arg^{172} in TM2 of VPAC2 (45). In the glucagon receptor, position 3 of glucagon (Gln^3) was predicted to be close to Ile^{194} in TM2 of the glucagon receptor (46–48). Although these data generally support that the amino-terminal region of the class B GPCR ligands resides within their receptor core, the details of the residue spatial approximation remain unclear until the structure of the receptor extracellular loops is resolved.

As we better understand the critical molecular interactions in this agonist pocket, it is likely that a variety of chemistries will be required to provide complementation and activation. Although the diversity of GLP-1 receptor small molecule agonists may seem to support this, it is not yet clear where they each might dock, and the possibility exists that these receptors can be activated by agents acting at a variety of sites, including the intracellular face of the receptor (49). The current work has provided new insights into the natural agonist binding pocket and a key interaction that may occur there. Higher resolution structures for receptors in this family, particularly as complexed with agonist ligands, will be critical to give us the same level of understanding for the class B GPCRs that we are beginning to appreciate for the class A GPCRs.

Author Contributions—M. D. and L. J. M. designed the study. M. D. performed the experiments and data analysis. P. C.-H. L. and A. O. performed molecular modeling. M. D., P. C.-H. L., P. M. S., A. C., R. A., and L. J. M. wrote the paper. All authors approved the final version of the manuscript.

Acknowledgments—We thank D. I. Pinon, A. S. Ball, and M. L. Augustine for excellent technical assistance.

References

1. Neumann, J. M., Couvineau, A., Murail, S., Lacapère, J. J., Jamin, N., and Laburthe, M. (2008) Class-B GPCR activation: is ligand helix-capping the key? *Trends Biochem. Sci.* **33,** 314–319
2. Miller, L. J., Dong, M., Harikumar, K. G., and Gao, F. (2007) Structural basis of natural ligand binding and activation of the Class II G-protein-coupled secretin receptor. *Biochem. Soc. Trans.* **35,** 709–712
3. Miller, L. J., and Dong, M. (2013) The orthosteric agonist-binding pocket in the prototypic class B G-protein-coupled secretin receptor. *Biochem. Soc. Trans.* **41,** 154–158
4. Ulrich, C. D., 2nd, Holtmann, M., and Miller, L. J. (1998) Secretin and vasoactive intestinal peptide receptors: members of a unique family of G protein-coupled receptors. *Gastroenterology* **114,** 382–397
5. Dong, M., Xu, X., Ball, A. M., Makhoul, J. A., Lam, P. C., Pinon, D. I., Orry, A., Sexton, P. M., Abagyan, R., and Miller, L. J. (2012) Mapping spatial approximations between the amino terminus of secretin and each of the extracellular loops of its receptor using cysteine trapping. *FASEB J.* **26,** 5092–5105
6. Yang, L., Yang, D., de Graaf, C., Moeller, A., West, G. M., Dharmarajan, V., Wang, C., Siu, F. Y., Song, G., Reedtz-Runge, S., Pascal, B. D., Wu, B., Potter, C. S., Zhou, H., Griffin, P. R., Carragher, B., Yang, H., Wang, M. W., Stevens, R. C., and Jiang, H. (2015) Conformational states of the full-length glucagon receptor. *Nat. Commun.* **6,** 7859
7. Castro, M., Nikolaev, V. O., Palm, D., Lohse, M. J., and Vilardaga, J. P. (2005) Turn-on switch in parathyroid hormone receptor by a two-step parathyroid hormone binding mechanism. *Proc. Natl. Acad. Sci. U.S.A.* **102,** 16084–16089
8. Gardner, J. D., Conlon, T. P., Beyerman, H. C., and Van Zon, A. (1977) Interaction of synthetic 10-tyrosyl analogues of secretin with hormone receptors on pancreatic acinar cells. *Gastroenterology* **73,** 52–56
9. Powers, S. P., Pinon, D. I., and Miller, L. J. (1988) Use of *N*,*O*-bis-Fmoc-D-Tyr-ONSu for introduction of an oxidative iodination site into cholecystokinin family peptides. *Int. J. Pept. Protein Res.* **31,** 429–434
10. Chen, Q., Pinon, D. I., Miller, L. J., and Dong, M. (2009) Molecular basis of glucagon-like peptide 1 docking to its intact receptor studied with carboxyl-terminal photolabile probes. *J. Biol. Chem.* **284,** 34135–34144
11. Harikumar, K. G., Pinon, D. I., and Miller, L. J. (2007) Transmembrane segment IV contributes a functionally important interface for oligomerization of the Class II G protein-coupled secretin receptor. *J. Biol. Chem.* **282,** 30363–30372
12. Munson, P. J., and Rodbard, D. (1980) Ligand: a versatile computerized approach for characterization of ligand-binding systems. *Anal. Biochem.* **107,** 220–239
13. Laemmli, U. K. (1970) Cleavage of structural proteins during the assembly of the head of bacteriophage T4. *Nature* **227,** 680–685
14. Abagyan, R., Totrov, M., and Kuznetsov, D. (1994) ICM-A new method for protein modeling and design: applications to docking and structure prediction from the distorted native conformation. *J. Comput. Chem.* **15,** 488–506
15. Parthier, C., Kleinschmidt, M., Neumann, P., Rudolph, R., Manhart, S., Schlenzig, D., Fanghänel, J., Rahfeld, J. U., Demuth, H. U., and Stubbs, M. T. (2007) Crystal structure of the incretin-bound extracellular domain of a G protein-coupled receptor. *Proc. Natl. Acad. Sci. U.S.A.* **104,** 13942–13947
16. Dong, M., Lam, P. C., Pinon, D. I., Hosohata, K., Orry, A., Sexton, P. M., Abagyan, R., and Miller, L. J. (2011) Molecular basis of secretin docking to its intact receptor using multiple photolabile probes distributed throughout the pharmacophore. *J. Biol. Chem.* **286,** 23888–23899
17. Harikumar, K. G., Lam, P. C., Dong, M., Sexton, P. M., Abagyan, R., and Miller, L. J. (2007) Fluorescence resonance energy transfer analysis of secretin docking to its receptor: mapping distances between residues distributed throughout the ligand pharmacophore and distinct receptor residues. *J. Biol. Chem.* **282,** 32834–32843
18. Siu, F. Y., He, M., de Graaf, C., Han, G. W., Yang, D., Zhang, Z., Zhou, C., Xu, Q., Wacker, D., Joseph, J. S., Liu, W., Lau, J., Cherezov, V., Katritch, V., Wang, M. W., and Stevens, R. C. (2013) Structure of the human glucagon class B G-protein-coupled receptor. *Nature* **499,** 444–449
19. Dong, M., Lam, P. C., Pinon, D. I., Sexton, P. M., Abagyan, R., and Miller, L. J. (2008) Spatial approximation between secretin residue five and the third extracellular loop of its receptor provides new insight into the molecular basis of natural agonist binding. *Mol. Pharmacol.* **74,** 413–422
20. Dong, M., Li, Z., Pinon, D. I., Lybrand, T. P., and Miller, L. J. (2004) Spatial approximation between the amino terminus of a peptide agonist and the top of the sixth transmembrane segment of the secretin receptor. *J. Biol. Chem.* **279,** 2894–2903
21. Hooft, R. W., Vriend, G., Sander, C., and Abola, E. E. (1996) Errors in protein structures. *Nature* **381,** 272–272
22. Garcia, G. L., Dong, M., and Miller, L. J. (2012) Differential determinants for coupling of distinct G proteins with the class B secretin receptor. *Am. J. Physiol. Cell Physiol.* **302,** C1202–C1212
23. Watkins, H. A., Au, M., and Hay, D. L. (2012) The structure of secretin family GPCR peptide ligands: implications for receptor pharmacology and drug development. *Drug Discov. Today* **17,** 1006–1014

24. Dong, M., Pinon, D. I., and Miller, L. J. (2013) Insights into the impact of phenolic residue incorporation at each position along secretin for receptor binding and biological activity. *Regul. Pept.* **180,** 5–11
25. Dong, M., Wang, Y., Hadac, E. M., Pinon, D. I., Holicky, E., and Miller, L. J. (1999) Identification of an interaction between residue 6 of the natural peptide ligand and a distinct residue within the amino-terminal tail of the secretin receptor. *J. Biol. Chem.* **274,** 19161–19167
26. Koth, C. M., Murray, J. M., Mukund, S., Madjidi, A., Minn, A., Clarke, H. J., Wong, T., Chiang, V., Luis, E., Estevez, A., Rondon, J., Zhang, Y., Hötzel, I., and Allan, B. B. (2012) Molecular basis for negative regulation of the glucagon receptor. *Proc. Natl. Acad. Sci. U.S.A.* **109,** 14393–14398
27. Wheatley, M., Wootten, D., Conner, M. T., Simms, J., Kendrick, R., Logan, R. T., Poyner, D. R., and Barwell, J. (2012) Lifting the lid on GPCRs: the role of extracellular loops. *Br. J. Pharmacol.* **165,** 1688–1703
28. Katritch, V., Cherezov, V., and Stevens, R. C. (2013) Structure-function of the G protein-coupled receptor superfamily. *Annu. Rev. Pharmacol. Toxicol.* **53,** 531–556
29. Donnelly, D. (1997) The arrangement of the transmembrane helices in the secretin receptor family of G-protein-coupled receptors. *FEBS Lett.* **409,** 431–436
30. Pal, K., Melcher, K., and Xu, H. E. (2012) Structure and mechanism for recognition of peptide hormones by Class B G-protein-coupled receptors. *Acta Pharmacol. Sin.* **33,** 300–311
31. Parthier, C., Reedtz-Runge, S., Rudolph, R., and Stubbs, M. T. (2009) Passing the baton in class B GPCRs: peptide hormone activation via helix induction? *Trends Biochem. Sci.* **34,** 303–310
32. Behar, V., Bisello, A., Bitan, G., Rosenblatt, M., and Chorev, M. (2000) Photoaffinity cross-linking identifies differences in the interactions of an agonist and an antagonist with the parathyroid hormone/parathyroid hormone-related protein receptor. *J. Biol. Chem.* **275,** 9–17
33. Hollenstein, K., Kean, J., Bortolato, A., Cheng, R. K., Doré, A. S., Jazayeri, A., Cooke, R. M., Weir, M., and Marshall, F. H. (2013) Structure of class B GPCR corticotropin-releasing factor receptor 1. *Nature* **499,** 438–443
34. Kruse, A. C., Ring, A. M., Manglik, A., Hu, J., Hu, K., Eitel, K., Hübner, H., Pardon, E., Valant, C., Sexton, P. M., Christopoulos, A., Felder, C. C., Gmeiner, P., Steyaert, J., Weis, W. I., Garcia, K. C., Wess, J., and Kobilka, B. K. (2013) Activation and allosteric modulation of a muscarinic acetylcholine receptor. *Nature* **504,** 101–106
35. Rasmussen, S. G., Choi, H. J., Fung, J. J., Pardon, E., Casarosa, P., Chae, P. S., Devree, B. T., Rosenbaum, D. M., Thian, F. S., Kobilka, T. S., Schnapp, A., Konetzki, I., Sunahara, R. K., Gellman, S. H., Pautsch, A., Steyaert, J., Weis, W. I., and Kobilka, B. K. (2011) Structure of a nanobody-stabilized active state of the β2 adrenoceptor. *Nature* **469,** 175–180
36. Rasmussen, S. G., DeVree, B. T., Zou, Y., Kruse, A. C., Chung, K. Y., Kobilka, T. S., Thian, F. S., Chae, P. S., Pardon, E., Calinski, D., Mathiesen, J. M., Shah, S. T., Lyons, J. A., Caffrey, M., Gellman, S. H., Steyaert, J., Skiniotis, G., Weis, W. I., Sunahara, R. K., and Kobilka, B. K. (2011) Crystal structure of the β2 adrenergic receptor-G_s protein complex. *Nature* **477,** 549–555
37. Scheerer, P., Park, J. H., Hildebrand, P. W., Kim, Y. J., Krauss, N., Choe, H. W., Hofmann, K. P., and Ernst, O. P. (2008) Crystal structure of opsin in its G-protein-interacting conformation. *Nature* **455,** 497–502
38. Willard, F. S., Bueno, A. B., and Sloop, K. W. (2012) Small molecule drug discovery at the glucagon-like peptide-1 receptor. *Exp. Diabetes Res.* **2012,** 709893
39. Dong, M., Le, A., Te, J. A., Pinon, D. I., Bordner, A. J., and Miller, L. J. (2011) Importance of each residue within secretin for receptor binding and biological activity. *Biochemistry* **50,** 2983–2993
40. Hefford, M. A., and Kaplan, H. (1989) Chemical properties of the histidine residue of secretin: evidence for a specific intramolecular interaction. *Biochim. Biophys. Acta* **998,** 267–270
41. Vilardaga, J. P., di Paolo, E., de Neef, P., Waelbroeck, M., Bollen, A., and Robberecht, P. (1996) Lysine 173 residue within the first exoloop of rat secretin receptor is involved in carboxylate moiety recognition of Asp-3 in secretin. *Biochem. Biophys. Res. Commun.* **218,** 842–846
42. Di Paolo, E., Petry, H., Moguilevsky, N., Bollen, A., De Neef, P., Waelbroeck, M., and Robberecht, P. (1999) Mutations of aromatic residues in the first transmembrane helix impair signalling by the secretin receptor. *Receptors Channels* **6,** 309–315
43. Di Paolo, E., De Neef, P., Moguilevsky, N., Petry, H., Bollen, A., Waelbroeck, M., and Robberecht, P. (1998) Contribution of the second transmembrane helix of the secretin receptor to the positioning of secretin. *FEBS Lett.* **424,** 207–210
44. Solano, R. M., Langer, I., Perret, J., Vertongen, P., Juarranz, M. G., Robberecht, P., and Waelbroeck, M. (2001) Two basic residues of the h-VPAC1 receptor second transmembrane helix are essential for ligand binding and signal transduction. *J. Biol. Chem.* **276,** 1084–1088
45. Vertongen, P., Solano, R. M., Perret, J., Langer, I., Robberecht, P., and Waelbroeck, M. (2001) Mutational analysis of the human vasoactive intestinal peptide receptor subtype VPAC(2): role of basic residues in the second transmembrane helix. *Br. J. Pharmacol.* **133,** 1249–1254
46. Perret, J., Van Craenenbroeck, M., Langer, I., Vertongen, P., Gregoire, F., Robberecht, P., and Waelbroeck, M. (2002) Mutational analysis of the glucagon receptor: similarities with the vasoactive intestinal peptide (VIP)/pituitary adenylate cyclase-activating peptide (PACAP)/secretin receptors for recognition of the ligand's third residue. *Biochem. J.* **362,** 389–394
47. Runge, S., Gram, C., Brauner-Osborne, H., Madsen, K., Knudsen, L. B., and Wulff, B. S. (2003) Three distinct epitopes on the extracellular face of the glucagon receptor determine specificity for the glucagon amino terminus. *J. Biol. Chem.* **278,** 28005–28010
48. Runge, S., Wulff, B. S., Madsen, K., Bräuner-Osborne, H., and Knudsen, L. B. (2003) Different domains of the glucagon and glucagon-like peptide-1 receptors provide the critical determinants of ligand selectivity. *Br J. Pharmacol.* **138,** 787–794
49. Nolte, W. M., Fortin, J. P., Stevens, B. D., Aspnes, G. E., Griffith, D. A., Hoth, L. R., Ruggeri, R. B., Mathiowetz, A. M., Limberakis, C., Hepworth, D., and Carpino, P. A. (2014) A potentiator of orthosteric ligand activity at GLP-1R acts via covalent modification. *Nat. Chem. Biol.* **10,** 629–631